Bioconjugate Chemistry

Article

Cite This: Bioconjugate Chem. 2020, 31, 241−247

pubs.acs.org/bc

Tailoring Kidney Transport of Organic Dyes with Low-Molecular-Weight PEGylation

Bujie Du,[†] Xingya Jiang,[†] Yingyu Huang,[†] Siqing Li,[†] Jason C Lin,[†] Mengxiao Yu,[†] and Jie Zheng*[,†]

[†]Department of Chemistry and Biochemistry, The University of Texas at Dallas, Richardson, Texas 75080, United States

Supporting Information

ABSTRACT: Subtle changes in size can induce distinct responses of the body to hard nanomaterials; however, it is largely unknown whether just a few ethylene oxide unit differences in soft poly(ethylene glycol) (PEG) molecules could significantly alter the renal clearance of small molecules. By systematically investigating in vivo transport of the representative renal clearable organic dyes, IRDye800CW after being conjugated with a series of PEG molecules with molecular weight (MW) below 10 kDa, we found a MW-dependent scaling law: PEG45 (MW = 2100 Da) is an optimized MW to generate the most efficient renal clearance for IRDye800CW by expediting the glomerular filtration of organic dyes and reducing their nonspecific interactions with background tissue. Moreover, the uniqueness of PEG45 can be generalized to other organic dyes such as ZW800-1 and fluorescein. This finding highlights the importance of low-MW PEGylation in tailoring in vivo transport of organic fluorophores, which would broaden their biomedical applications.

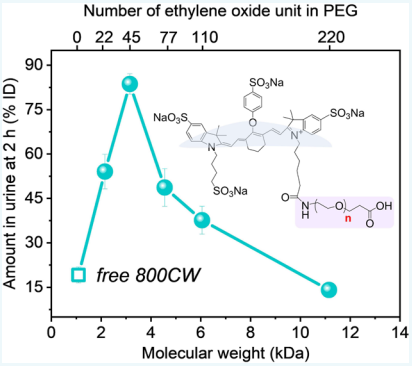

INTRODUCTION

Unravelling distinct responses of the body to subtle differences among ultrasmall hard or soft engineered materials is not only fundamentally important to understanding physiology at the nanoscale, but also critical to precise control of their functionalities and toxicities.[1,2] In the past decades, significant efforts have been dedicated to studying the response of the body to hard engineered nanoparticles and discovering many size dependencies in both clearance and disease targeting. For instance, Chan[3] et al. found that tumor targeting efficiencies of engineered gold nanoparticles are strongly size dependent and observed an optimal size window of 60 nm for efficient tumor targeting. Choi[4] et al. observed a size threshold of ∼5.5 nm for glomerular filtration of quantum dots. In 2017, our group observed an inverse size-dependent glomerular filtration of gold nanoclusters in a sub-nanometer regime, where only a 7-gold atom difference in cluster size can induce significant changes in their glomerular filtration.[5] Against the prevailing understanding that smaller particles are filtered faster than large ones, we found that the glomerular filtration exponentially decreased with the reduction of number of gold atoms once the cluster size was below 1 nm. These studies clearly indicate that our body is highly sensitive to seemingly trivial differences among hard engineered nanoparticles, particularly in a small size range. Since soft materials also play a key role in disease diagnosis and treatment,[6−10] a fundamental question naturally emerges regarding whether the body also exhibits distinct responses to ultrasmall soft materials with subtle differences in molecular weight.

PEGylation is the most widely used bioconjugation chemistry in the medical industry,[11−13] because the biocompatibility, amphiphilicity, and tunable size of polyethylene glycol (PEG) molecules could render parent molecules unique in vivo transport and interactions.[14] PEG molecules are known to exhibit size-dependent glomerular filtration:[14,15] PEG molecules with MW between 1500 and 4000 Da are known to rapidly clear through the glomerular filtration membranes,[16] whereas larger PEG molecules with MW in the range of 6000−40 000 Da have stronger interaction with the glomerular filtration membrane, resulting in their slower renal clearance efficiency.[16,17] For example, PEG10 kDa, PEG20 kDa, and PEG40 kDa are cleared into urine at 24 h post-injection with the reducing renal clearance efficiencies of 44.1% ID, 42.4% ID, and 14.7% ID, respectively.[18] Because of these, PEGylation has been a simple and widely used chemistry to tailor the blood retention and clearance kinetics of small molecules.[18−20] For example, the conjugation of a single PEG with MW larger than 20 kDa to indocyanine green (ICG) remarkably increased its blood retention.[18] However, PEGylation with MW below 10 kDa failed to significantly enhance the blood retention of organic molecules due to its fast glomerular filtration. For instance, the conjugation of one PEG of 2000 Da only increased the blood retention of zidovudine by 15%.[19] Until now, it has been generally accepted that bulky sizes of PEG molecules with high molecular weights (MW > 10 000 Da) effectively prevent rapid renal clearance of small molecules by significantly increasing size, while low-MW PEGylation makes trivial contributions in tailoring the renal clearance of small molecules in comparison with high MW PEGylation counter-

Special Issue: Molecular Imaging

Received: October 19, 2019
Revised: November 4, 2019
Published: November 7, 2019

DOI: 10.1021/acs.bioconjchem.9b00707
Bioconjugate Chem. 2020, 31, 241−247

parts.[15,18,21−23] However, systematic investigation on the size effect of sub-10 kDa PEGylation on renal clearance of small molecules is still lacking. Moreover, the observation of highly sensitive body responses to ultrasmall hard engineered nanoparticles inspires us to revisit the impacts of low-molecular-weight PEGylation on the renal clearance of small molecules: (1) Can the body differentiate molecules conjugated with different-sized PEG with MW below 10 000 Da? (2) How can the low-MW PEGylation affect the renal clearance of small molecules?

To answer these questions and broaden the potential biomedical applications of low-MW PEGylated small molecules, we chose a representative near-infrared (NIR)-emitting organic dye, IDye800CW (abbreviated as 800CW), as the parent molecule, because it resists serum protein binding and is eliminated through the glomeruli into the urine, the same clearance route taken by PEG molecules. In addition, ZW800-1, the NIR organic dye reported by Choi's group,[24] was also selected to be parent molecule, since it displays fewer nonspecific interactions with background tissue and higher clearance than IRDye800CW[24] because of its zwitterionic property. One representative visible renal clearable dye, fluorescein, was also included due to its broad biomedical applications. By quantifying the renal clearance of after being conjugated with low-MW PEG molecules, we found that these PEGylated organic dyes follow a general MW-dependent scaling law in which PEG45 (MW = 2100 Da) is an optimized MW to generate the most efficient renal clearance for organic dyes. The PEG45 not only significantly accelerated the glomerular filtration of 800CW but also reduced its nonspecific interactions with background tissue, resulting in noninvasive observation of the kidneys by 800CW-PEG45. The uniqueness of PEG45 in tailoring the kidney transport of 800CW can also be generalized into ZW800-1 and fluorescein. This finding highlights the precise responses of the body to soft nanomaterials and the importance of low-MW PEGylation in tailoring the transport of organic dyes, which will broaden the biomedical applications of organic dyes in detection of renal disease.

RESULTS AND DISCUSSION

We first investigated the sub-10 kDa PEGylation effect on the clearance percentage of renal clearable IRDye800CW in the urine. The synthesis of IRDye800CW-PEG*n* (abbreviated as 800CW-PEG*n*; *n* represents the number of repeat ethylene oxide units in PEG), including 800CW-PEG22, 800CW-PEG45, 800CW-PEG77, 800CW-PEG110, and 800CW-PEG220, was readily achieved through the reaction between the *N*-hydroxysuccinimide (NHS) ester of preactivated IRDye800CW and the amine group of PEG molecules (Figure S1). The successful conjugation of different MW PEG molecules to IRDye800CW was confirmed by their different mobility in agarose gel (Figure S2). The obtained 800CW-PEG*n* inherit absorption and emission spectra of free IRDye800CW (Figure S3), which allows us to quantitatively in situ monitor their clearance in vivo. Due to the hydrophilicity of IRDye800CW and the amphiphilicity of PEG molecules, the hydrophobic character (partition coefficient, log*D*) at pH 7.4 of 800CW-PEG*n* are comparable (Figure 1a), and they all resist serum proteins (Figure S4). Also, the net charge of 800CW-PEG*n* was kept same before and after PEGylation (Figure 1a; the chemical structure of free IRDye800CW is in Figure S1), which allow us to correlate

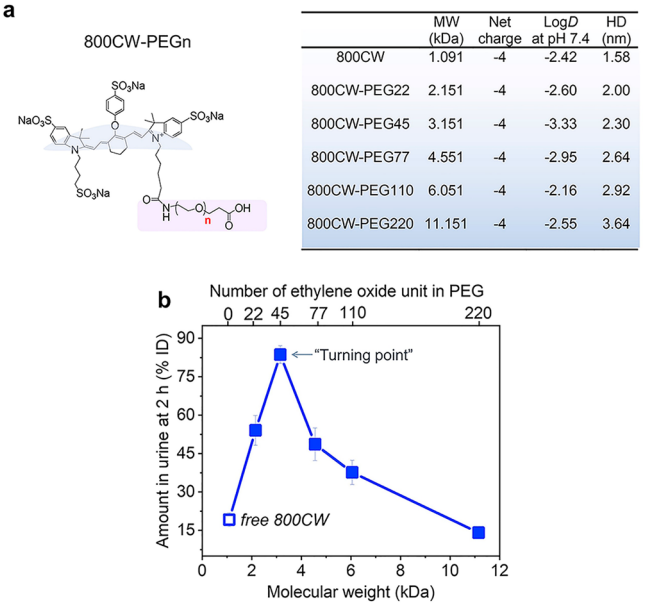

	MW (kDa)	Net charge	Log*D* at pH 7.4	HD (nm)
800CW	1.091	-4	-2.42	1.58
800CW-PEG22	2.151	-4	-2.60	2.00
800CW-PEG45	3.151	-4	-3.33	2.30
800CW-PEG77	4.551	-4	-2.95	2.64
800CW-PEG110	6.051	-4	-2.16	2.92
800CW-PEG220	11.151	-4	-2.55	3.64

Figure 1. Sub-10 kDa PEGylation effect on renal clearance of IRDye800CW. a. Chemical structure, molecular weight (MW), net charge, hydrophobic character (partition coefficient, log*D* at pH 7.4, experimentally measured), as well as hydrodynamic diameter (HD, calculated based on empirical equation of folded molecules, which is described in Experimental Procedure) of free IRDye800CW (800CW) and PEGylated 800CW. b. Renal clearance efficiencies of 800CW, 800CW-PEG22, 800CW-PEG45, 800CW-PEG77, 800CW-PEG110, and 800CW-PEG220 at 2 h post-intravenous injection (n = 3, mean ± s.d.) versus molecular weight. PEG45 is an optimized size for renal clearance of 800CW-PEG*n*.

their renal clearance efficiencies with their molecular weight. By systematically quantifying the amount of 800CW and 800CW-PEG*n* in the urine 2 h post-intravenous injection (p.i.), we found that only an ~1 kDa difference in the MW of PEG molecules can result in distinct renal clearance efficiency: 19.2% ID (percentage of injection dose), 54.1% ID, 83.7% ID, 48.7% ID, 37.7% ID, and 14.1% ID of 800CW, 800CW-PEG22, 800CW-PEG45, 800CW-PEG77, 800CW-PEG110, and 800CW-PEG220 were cleared into urine at 2 h p.i., respectively. Consistent with conventional understanding, PEGylation with MW above 10 kDa rendered slow kidney transport of parent small molecules due to the size-dependent renal clearance of bulky PEG molecules. Counterintuitively to the prevailing understanding that larger PEGylation more easily reduces the glomerular filtration of parent small molecules than smaller ones, we found a unique MW-dependent scaling law of PEGylation with MW below 10 kDa: once a PEG ligand is smaller than PEG45, smaller conjugates are eliminated more slowly; however, once the PEG ligand is larger than PEG45, larger ones are cleared more slowly into the urine (Figure 1b), clearly showing that the PEG45 is an optimum one for efficient renal clearance of 800CW.

To further understand the in vivo behaviors of 800CW-PEG*n*, we conducted the blood pharmacokinetics of free 800CW, 800CW-PEG22, 800CW-PEG45, and 800CW-PEG220 (Figure 2a). Although these four small molecules displayed two-compartment pharmacokinetics, the 800CW-PEG45 exhibited the shortest blood retention, followed by 800CW-PEG22, 800CW, and 800CW-PEG220. From these

DOI: 10.1021/acs.bioconjchem.9b00707
Bioconjugate Chem. 2020, 31, 241−247

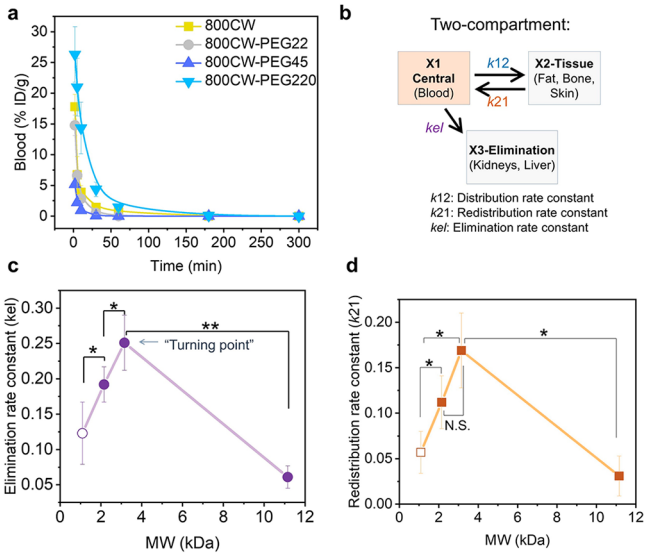

Figure 2. Sub-10 kDa PEGylation effect on pharmacokinetics of IRDye800CW. a. Blood pharmacokinetics of free 800CW, 800CW-PEG22, 800CW-PEG45, and 800CW-PEG220. (n = 3, mean ± s.d.). b. Diagram of two-compartment model of pharmacokinetics. c. Elimination rate constant (k_{el}) of free 800CW, 800CW-PEG22, 800CW-PEG45, and 800CW-PEG220 versus molecular weight (MW). d. Redistribution rate constant of free 800CW, 800CW-PEG22, 800CW-PEG45, and 800CW-PEG220 versus MW. *P < 0.05, **P < 0.005, Student's t test.

two-compartment pharmacokinetics, we are able to derive three important factors, k_{el} (elimination rate constant, a parameter that reflects the extent of the body in eliminating exogenous substances), k_{12} (distribution rate constant from central compartment to peripheral compartment), and k_{21} (redistribution rate constant from peripheral compartment to central compartment) (Figure 2b). As shown in Figure 2c, 800CW-PEG45 exhibited the largest k_{el}, which is ~2 times, ~1.3 times, and ~4 times higher than the k_{el} values of 800CW, 800CW-PEG22, and 800CW-PEG45, respectively, clearly showing the uniqueness of PEG45 in acceleration of 800CW transport in the kidneys, consistent with the results of renal clearance efficiency. The conjugation of PEG molecules with MW below 10 kDa remained the k_{12} values of 800CW from blood to background tissue (Figure S5) but significantly improved the k_{21} of 800CW (Figure 2d), indicating that linking of PEG22 and PEG45 to 800CW significantly facilitates the intravasation but has little effect on the extravasation of 800CW. By analyzing these results, we concluded that PEG22 and PEG45 equally (2−3 times) reduced the nonspecific interaction of 800CW while PEG45 more obviously promoted the clearance of 800CW than PEG22. Compared with PEG22 and PEG45, 800CW-PEG220 is more difficultly cleared through the kidneys due to its larger size. Thus, the observed highest renal clearance efficiency of 800CW-PEG45 is mainly attributed to its fastest transport in the kidneys among these 800CW-PEGn. In addition, 800CW-PEG45 also acts as the turning point in the pharmacokinetics parameters, CL (clearance), $T_{1/2}$ (elimination half-life), volume distribution (Vd), and AUC (area under the curve) (Table 1 and Figure S6), implying that the trivial change in molecular size of PEGylated 800CW leads to a broad impact on the in vivo transport.

The fast kidney transport and reduced nonspecific interactions enable 800CW-PEG45 to noninvasively light up the kidneys with high contrast index. As shown in Figure 3a, by noninvasively and fluorescently imaging the kidneys of mice injected with free 800CW or 800CW-PEG45 at different time points post-injection (Figure 3a), we observed distinct time-dependent fluorescence intensity curves between them (Figure 3b). The signals of 800CW from the kidneys are quickly overshadowed by the signal from the background tissue, resulting in indiscernability of the kidneys. In contrast, the signal of 800CW-PEG45 from the kidneys is much higher than that of background tissue, resulting in the kidney contrast index at 5 min p.i. being ~3.4 times higher than that of 800CW (Figure 3b). Additionally, the fluorescent signal of 800CW-PEG45 in the kidneys displays a rapid decrease after reaching its maximum within 30 min. Such rapid kidney transport of 800CW-PEG45 results in strong fluorescent signal of 800CW-PEG45 in the bladder at 30 min (Figure 3c) and its minor accumulation in other organs, such as the liver, spleen, and heart, which implies a small interaction of 800CW-PEG45 in the body. Furthermore, we found that the fast kidney clearance of 800CW-PEG45 is attributed to its fast glomerular filtration by harvesting the kidneys from the mice injected with 800CW-PEG45 at 5 min and 1 h p.i. for H&E staining to locate its distribution in the kidneys at the tissue level. The fluorescent signals of 800CW-PEG45 in the glomerulus and proximal tubular lumen were clearly detected at 5 min p.i. (Figure 3d), indicating that 800CW-PEG45 was filtered through the glomerulus into the tubular lumen. The rapid renal clearance of 800CW-PEG45 resulted in a very weak signal from the kidneys at 1 h p.i. (Figure S7).

Not limited to IRDye800CW, PEG45 also facilitated the renal clearance of other organic dyes. ZW800-1 (Figure 4a), the NIR organic dye reported by Choi's group,[24] displays fewer nonspecific interactions with background tissue and higher clearance than IRDye800CW[24] (Figure S8) due to its zwitterionic property. While ZW800-1 is cleared very fast through the kidneys, the conjugation of PEG45 further facilitated its kidney transport in the kidneys which was proved by the comparison of k_{el} (Figure 4b) derived from their

Table 1. Pharmacokinetics Parameters of 800CW-PEGn

	800CW	800CW-PEG22	800CW-PEG45	800CW-PEG220
k_{el} (min^{-1})	0.123 ± 0.044	0.192 ± 0.025	0.251 ± 0.039	0.061 ± 0.016
CL (mL/min)	0.54 ± 0.10	1.12 ± 0.09	4.05 ± 0.93	0.23 ± 0.06
$T1/2$ (min)	4.03 ± 1.35	2.26 ± 0.25	1.50 ± 0.08	10.30 ± 2.41
Vd (mL)	3.04 ± 0.42	3.64 ± 0.47	8.84 ± 2.41	3.24 ± 0.68
AUC (min %ID/g)	188.63 ± 37.69	89.20 ± 6.39	25.53 ± 5.57	468.57 ± 140.91
k_{12} (min^{-1})	0.190 ± 0.089	0.145 ± 0.040	0.155 ± 0.084	0.028 ± 0.020
k_{21} (min^{-1})	0.057 ± 0.023	0.112 ± 0.029	0.169 ± 0.041	0.031 ± 0.022

DOI: 10.1021/acs.bioconjchem.9b00707
Bioconjugate Chem. 2020, 31, 241−247

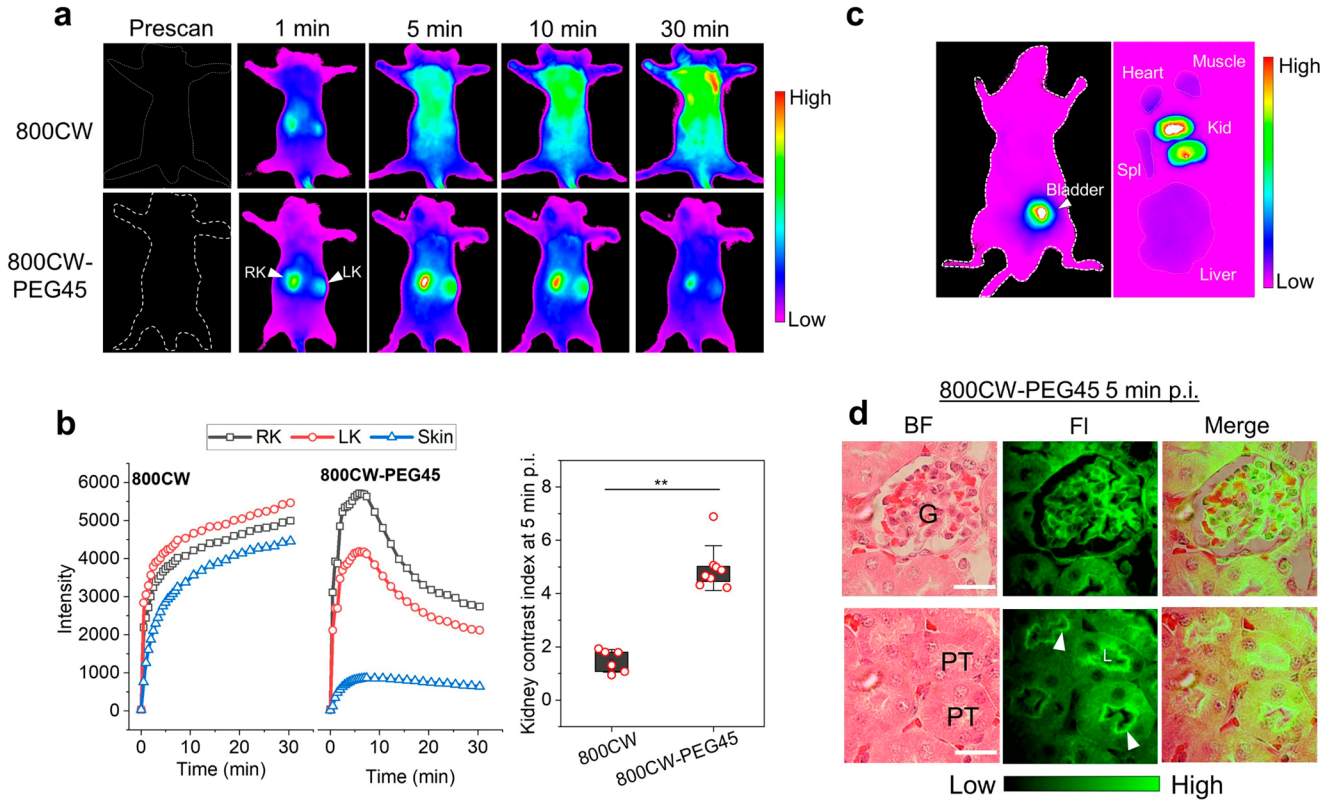

Figure 3. Real-time imaging of transport of 800CW-PEG45 in the kidneys as well as its localization in the kidney at tissue level. a. Real-time noninvasive kidney imaging before and after intravenous injection of 800CW-PEG45 (Ex/Em filters: 720/790 nm). The mouse was placed in supine position on the imaging stage. b. Time−fluorescence intensity curves of two kidneys and background skin within 30 min post-injection of 800CW and 800CW-PEG45 as well as the kidney contrast index at 5 min post-injection. *P < 0.05, **P < 0.005, Student's t test. c. Signal of 800CW-PEG45 in bladder at 30 min (the mouse was placed in prone position) and ex vivo images of harvested kidneys (Kid), liver, spleen (Spl), heart, and muscle at 30 min post-injection. d. Fluorescence images of glomerulus and tubules at tissue level at 5 min post-injection of 800CW-PEG45. G, glomerulus; PT, proximal tubule. Kidney tissue was stained by Hematoxylin and Eosin (H&E) stain. Fluorescence images were taken at 720/790 nm. Scalar bar is 20 μm.

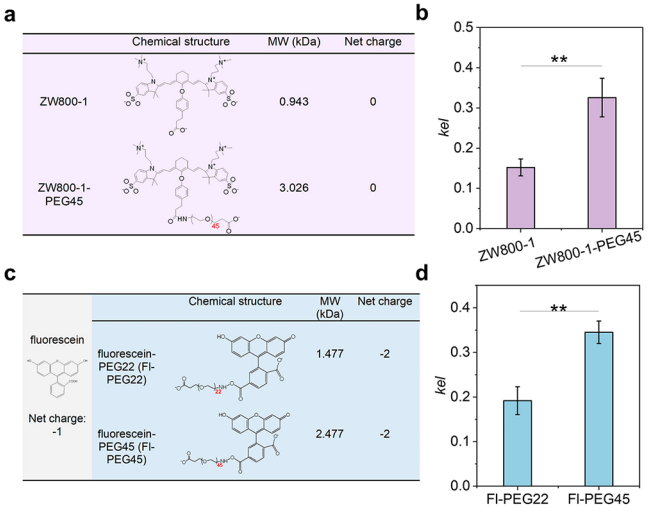

Figure 4. Generalization of PEG45 to other organic dyes in tuning renal clearance. a. Chemical structures, molecular weight (MW), and net charge of ZW800-1 and ZW800-1-PEG45. b. Comparison between k_{el} of ZW800-1 and ZW800-1-PEG45. c. Chemical structures, MW, and net charge of Fl-PEG22 and Fl-PEG45. d. Comparison between k_{el} of Fl-PEG22 and Fl-PEG45. *P < 0.05, **P < 0.005, Student's t test.

pharmacokinetics (Figure S9). Although free ZW800-1 is cleared faster than free IRDye800CW through the kidneys, the conjugation of PEG45 to them result in comparable elimination rate constant (Figure S12). In addition to NIR dyes, we also chose one visible dye, fluorescein. The net charge of fluorescein is −1, while PEGylation altered its charge from −1 to −2 (Figure 4c); thus, we compared same-charged fluorescein-PEG22 (fl-PEG22) and fluorescein-PEG45 (fl-PEG45) instead of free fluorescein with fl-PEG45. As shown in Figure 4d, the PEG45 conjugation more easily assistes fluorescein to be cleared into urine than PEG22 conjugation (pharmacokinetics curves in Figure S10). Moreover, the elimination rate constant of fl-PEG45 is comparable with that of ZW800-1-PEG45 (Figure S12), indicating that the conjugation of PEG45 to renal clearable dyes resulted in comparable renal clearance. The magnitude change of orgainc dyes in renal clearance efficiency before and after conjugation with PEG45 is dependent of the intrinsic properties of organic dyes; however, after low-MW PEGylation, their renal clearance became comparable, indicating the important role of low-MW PEG molecules played in tuning the renal clearance of organic dyes. Besides, these results also clearly demonstrate the sensitivity of the kidneys in elimination of renal-clearable organic dyes after being conjugated with PEG molecules with MW below 10 kDa as well as an optimum PEG molecule for highly efficient renal clearance.

DOI: 10.1021/acs.bioconjchem.9b00707
Bioconjugate Chem. 2020, 31, 241−247

CONCLUSION

In summary, by systematically investigating in vivo transport of IRDye800CW conjugated with a series of low-MW PEG molecules (<10 000 Da), we found that just a ∼20-unit difference in length of PEG molecules can induce significant changes to parent dyes in their clearance kinetics and efficiency, clearly indicating the sensitive and precise responses of the body to seemingly trivial differences among ultrasmall soft materials. The observation of the MW-dependent scaling law in renal clearance of PEGylated dyes showed that there is an optimized MW of PEG (PEG45) for small molecules to achieve most efficient renal clearance efficiency, which further emphasized the necessities of precise control of PEGylation length in tuning clearance. Since 800CW-PEG45 is highly biocompatible, easily synthesized, strongly fluorescent, and cleared rapidly into urine with clear clearance mechanisms, it is promising in detecting kidney-related diseases by noninvasively monitoring its transport in the kidneys, as the role of ultrasmall glutathione-coated gold nanoparticles[25,26] and organic nanoparticles[27] played in renal disease detection. Moreover, 800CW-PEG45 could be used to measure the glomerular filtration rate since it is freely filtered through glomeruli, like FITC-inulin[28] (the gold standard in quantification of GFR), by blood testing or by photoacoustic imaging[29] due to the absorption of 800CW-PEG45 at 790 nm. The combination of all these results highlights the importance of precise control of small molecule transport in the kidneys with low MW PEGylation, which could open a new path to significantly broaden their biomedical applications.

EXPERIMENTAL PROCEDURE

Materials and Equipment. PEG samples with average molecular weights of 1100, 2100, 3500, 5000, and 10 100 Da were purchased from Sigma-Aldrich (USA). IRDye800CW-NHS and fluorescein-NHS were purchased from LI-COR. ZW800-1 NHS was purchased from Curadel. Absorption spectra were measured by a Virian 50 Bio UV−vis spectrophotometer. Fluorescence spectra were acquired by a PTI QuantaMaster 30 Fluorescence Spectrophotomer (Birmingham, NJ). In vivo fluorescence images were recorded using a Carestream In-vivo FX Pro imaging system. Optical images of cultured cells and tissue slides were obtained with an Olympus IX-71 inverted fluorescence microscope coupled with Photon Max 512 CCD camera (Princeton Instruments). Agarose gel electrophoresis was carried out by a Bio-Rad Mini-Sub Cell GT system. Animal studies were performed according to the guidelines of the University of Texas System Institutional Animal Care and Use Committee. BALB/c mice (BALB/cAnNCr, strain code 047) of 6−8 weeks old, weighing 20−25 g, were purchased from Envigo. All of these mice were randomly allocated and housed under standard environmental conditions (23 ± 1 °C, 50 ± 5% humidity, and a 12/12 h light/dark cycle) with free access to water and standard laboratory food.

Synthesis of 800CW-PEG Conjugates. 400 μL, 10 mM PEG molecules in ultrapure water were added into 400 μL, 400 μM IRDye800CW-NHS in DMSO and the mixture was vortexed for 3 h. Then, 800CW-PEG conjugates were purified with 2% agarose gel electrophoresis from free 800CW dye and PEG molecules based on their different mobility from free 800CW. Meanwhile, the different mobilities in agarose gel proved the successful synthesis of 800CW-PEG conjugates. The ZW800-1-PEG45 and Fl-PEG22 and Fl-PEG45 were synthesized by the same method with 800CW-PEG*n* through the reaction between of the preactivated ZW800-1-NHS and fluorescein-NHS with the carboxylic group of PEG molecules.

Serum Protein Binding Test. The protein binding of 800CW and 800CW-PEG*n* was also tested by quantifying their fluorescence intensity in water and in 100% FBS. The fluorescence images were taken by Carestream In-vivo FX Pro imaging system under 710 nm/790 nm.

Partition Coefficient Measurement. The partition coefficients (log*D*) at pH 7.4 of free IRDye800CW and 800CW-PEG conjugates were quantified by measuring their distribution in 1-octanol and phosphate-buffered saline (PBS) in the previously reported method.[30] Each organic dye was dissolved in the mixture of PBS and PBS saturated 1-octonal (v/v = 1:1), followed by shaking for 1 h by a rotatable mixer to allow organic dyes to reach the distribution equilibrium in these two different solvents. After that, the 1-octanol and PBS were separated by centrifuge at 10.00g for 3 min. Finally, the concentrations of organic dyes in each solvent were quantified by UV−vis spectroscopy.

Hydrodynamic Diameter Calculation. The hydrodynamic diameter (HD) of PEGylated organic dyes were calculated using the reported empirical equation which illustrated the relationship between molecular weight with hydrodynamic radius[31,32] (Supporting Information Figure 11) for unfolded and folded molecules. We utilized this empirical equation to calculate the HD of PEGylated 800CW and presented them in Figure 1a. This equation only described the HDs of molecules in PBS or in protein-free environment.

Renal Clearance Efficiencies of 800CW-PEG Conjugates. BALB/c mice were intravenously injected with 800CW (n = 3) and 800CW-PEG conjugates (n = 3 for each conjugate), respectively, with concentration of 40 μM and injection volume of 200 μL and then placed in metabolism cages. Mouse urine from 800CW, 800CW-PEG22, 800CW-PEG45, 800CW-PEG77, 800CW-PEG110, and 800CW-PEG220 were collected at 2 h post injection. Then, the urine was quantified based on fluorescence and each standard curve of conjugates were built in control urine. The detailed quantification method was described in Scheme S1 by taking 800CW as an example.

Noninvasive Fluorescence Imaging of Kidney with 800CW-PEG45. The bald BALB/c mouse was anesthetized using 3% isoflurane, and a catheter filled with PBS was inserted into the tail vein. The mouse with tail vein catheter was placed in a supine position on the imaging stage of Carestream In-vivo FX Pro imaging system, allowing the back to face the excitation light and CCD camera. The mouse with a steady breath rate of 10−14 times per 15 s was injected with PBS solution of 800CW-PEG45 (200 μL, 40 μM), and then sequential time-series imaging (10 s exposure) was carried out with Ex710/Em790 nm.

Kidney Images with Optical Microcopy. BALB/c mice were sacrificed at 5 min and 1 h after intravenous administration of 200 μL, 400 μM of 800CW-PEG45. The kidneys were then collected and fixed immediately in 10% neutral buffered formalin, followed by standard dehydration and paraffin embedding. The embedded tissues were then sectioned into 4 μm slices and H&E stained. The final slides were visualized under an Olympus IX-71 fluorescence microscope. The filters used for 800CW-PEG45 were Ex747/Em780LP and dichroic mirror 776 nm.

DOI: 10.1021/acs.bioconjchem.9b00707
Bioconjugate Chem. 2020, 31, 241−247

Pharmacokinetics Studies. BALB/c mice (n = 3 for each molecule) were intravenously injected with 800CW, 800CW-PEG22, 800CW-PEG45, and 800CW-PEG220 with concentration of 40 μM, 200 μL, respectively. Then, ~30 μL blood samples were collected from retro-orbital site at 2, 5, 10, and 30 min, and 1, 3, 5, 8, 10, 24 h post-injection. The blood samples were weighed and completely lysed in freshly made lysis buffer and then quantified based on fluorescence. Each standard curve of molecule was built in control blood.

Pharmacokinetics Parameters Calculation. The pharmacokinetics of free organic dyes and PEGylated organic dyes were plotted using OriginLab and fitted by a two-compartment exponential decay function (ExpDec2) of $y = A_1 \exp(-x/t_1) + A_2 \exp(-x/t_2) + y_0$, where x = time (min) and y was organic dye amount in blood (% ID/g, percentage of injected dose per gram of blood).

1. Calculation of k_{12}, k_{21}, and k_{el}. From the two-compartment exponential decay function, we got four values, A_1, A_2, $\alpha = 1/t_1$, $\beta = 1/t_2$. k_{21}, k_{12}, and k_{el} were calculated using following equations as reported:[17]

a. $k_{21} = (A_1 \cdot \beta + A_2 \cdot \alpha)/(A_1 + A_2)$

b. $k_{el} = (\alpha \cdot \beta)/k_{21}$

c. $k_{12} = \alpha + \beta - k_{21} - k_{el}$

2. Vd, $t_{1/2}$, and CL were calculated using following equations. a. $C_0 = A_1 + A_2 + y_0$

b. $Vd = 100/C_0$

c. $t_{1/2} = 0.693AUC/C_0$, where AUC was the integration of the pharmacokinetics

d. $CL = 100/AUC$

Statistical Analysis. Error bars are reported as mean ± s.d. The differences between groups were compared by analysis of Student's t test. P-value <0.05 was considered to be statistically significant. N.S. means no significant difference with p value >0.05. Investigators conducting the experiments were not blinded.

■ ASSOCIATED CONTENT

Supporting Information

The Supporting Information is available free of charge on the ACS Publications website at DOI: 10.1021/acs.bioconjchem.9b00707.

Synthesis, chemical structure, UV-vis absorption and fluorescence spectra, $k12$ and $k21$, and pharmakinetic parameters of 800CW-PEGn; Mobility of 800CW-PEGn in agarose gel; Protein binding test of 800CW-PEGn; Method to quantify renal clearance efficiency of organic dyes; 800CW-PEG45 distribution in the kidneys at 1 h post-injection; Pharmakinetics of ZW800-1, ZW800-1-PEG45, FL-PEG22, and FL-PEG45; Relationship between molecular weight with hydrodynamic radius of folded molecule (PEG) and unfolded protein; Comparison of elimination rate constants among 800CW-PEG45, ZW800-1-PEG45, and fluorescine-PEG45 (PDF)

■ AUTHOR INFORMATION

Corresponding Author

*E-mail: jiezheng@utdallas.edu.

ORCID

Jie Zheng: 0000-0001-8546-1882

Author Contributions

J.Z. conceived the idea and designed the experiments with B.D. B.D. conducted the experiments with the assistance of X.J., Y.H., and J.L. S.L. and M. Y. conducted the logD measurement. B.D. discussed and analyzed the results with J.Z. J.Z. and B.D. composed the manuscript. All authors commented on the manuscript.

Notes

The authors declare no competing financial interest.

■ ACKNOWLEDGMENTS

This work was supported by the NIH (R01DK103363 and R01DK115986), Welch Research Foundation (AT-1974-20180324) and Cecil H. and Ida Green Professorship of J.Z. from the University of Texas at Dallas.

■ REFERENCES

(1) Du, B., Yu, M., and Zheng, J. (2018) Transport and interactions of nanoparticles in the kidneys. *Nature Reviews Materials 3* (10), 358−374.

(2) Jiang, X., Du, B., Huang, Y., and Zheng, J. (2018) Ultrasmall noble metal nanoparticles: Breakthroughs and biomedical implications. *Nano Today 21*, 106−125.

(3) Sykes, E. A., Chen, J., Zheng, G., and Chan, W. C. (2014) Investigating the impact of nanoparticle size on active and passive tumor targeting efficiency. *ACS Nano 8* (6), 5696−5706.

(4) Soo Choi, H., Liu, W., Misra, P., Tanaka, E., Zimmer, J. P, Itty Ipe, B., Bawendi, M. G, and Frangioni, J. V (2007) Renal clearance of quantum dots. *Nat. Biotechnol. 25* (10), 1165−1170.

(5) Du, B., Jiang, X., Das, A., Zhou, Q., Yu, M., Jin, R., and Zheng, J. (2017) Glomerular barrier behaves as an atomically precise bandpass filter in a sub-nanometre regime. *Nat. Nanotechnol. 12* (11), 1096.

(6) Pu, K., Shuhendler, A. J., Jokerst, J. V., Mei, J., Gambhir, S. S., Bao, Z., and Rao, J. (2014) Semiconducting polymer nanoparticles as photoacoustic molecular imaging probes in living mice. *Nat. Nanotechnol. 9* (3), 233.

(7) Shuhendler, A. J., Pu, K., Cui, L., Uetrecht, J. P., and Rao, J. (2014) Real-time imaging of oxidative and nitrosative stress in the liver of live animals for drug-toxicity testing. *Nat. Biotechnol. 32* (4), 373.

(8) Zhang, Q., Dehaini, D., Zhang, Y., Zhou, J., Chen, X., Zhang, L., Fang, R. H., Gao, W., and Zhang, L. (2018) Neutrophil membrane-coated nanoparticles inhibit synovial inflammation and alleviate joint damage in inflammatory arthritis. *Nat. Nanotechnol. 13*, 1182.

(9) Hu, Q., Sun, W., Wang, J., Ruan, H., Zhang, X., Ye, Y., Shen, S., Wang, C., Lu, W., Cheng, K., et al. (2018) Conjugation of haematopoietic stem cells and platelets decorated with anti-PD-1 antibodies augments anti-leukaemia efficacy. *Nature Biomedical Engineering 2* (11), 831.

(10) Huynh, E., Leung, B. Y., Helfield, B. L., Shakiba, M., Gandier, J.-A., Jin, C. S., Master, E. R., Wilson, B. C., Goertz, D. E., and Zheng, G. (2015) In situ conversion of porphyrin microbubbles to nanoparticles for multimodality imaging. *Nat. Nanotechnol. 10* (4), 325.

(11) Miao, Q., Xie, C., Zhen, X., Lyu, Y., Duan, H., Liu, X., Jokerst, J. V., and Pu, K. (2017) Molecular afterglow imaging with bright, biodegradable polymer nanoparticles. *Nat. Biotechnol. 35* (11), 1102.

(12) Schipper, M. L., Iyer, G., Koh, A. L., Cheng, Z., Ebenstein, Y., Aharoni, A., Keren, S., Bentolila, L. A., Li, J., and Rao, J. (2009) Particle size, surface coating, and PEGylation influence the biodistribution of quantum dots in living mice. *Small 5* (1), 126−134.

(13) Lovell, J. F., Liu, T. W., Chen, J., and Zheng, G. (2010) Activatable photosensitizers for imaging and therapy. *Chem. Rev. 110* (5), 2839−2857.

(14) Harris, J. M., and Chess, R. B. (2003) Effect of pegylation on pharmaceuticals. *Nat. Rev. Drug Discovery 2* (3), 214−222.

DOI: 10.1021/acs.bioconjchem.9b00707
Bioconjugate Chem. 2020, 31, 241−247

(15) Li, W., Zhan, P., De Clercq, E., Lou, H., and Liu, X. (2013) Current drug research on PEGylation with small molecular agents. *Prog. Polym. Sci. 38* (3−4), 421−444.
(16) Jorgensen, K., Møller, J., and Sheikh, M. (1972) The glomerular filterability of inulin and of different molecular weight preparations of polyethylene glycol in the rabbit. *Acta Physiol. Scand. 84* (3), 408−414.
(17) Yamaoka, T., Tabata, Y., and Ikada, Y. (1994) Distribution and tissue uptake of poly (ethylene glycol) with different molecular weights after intravenous administration to mice. *J. Pharm. Sci. 83* (4), 601−606.
(18) Kanazaki, K., Sano, K., Makino, A., Yamauchi, F., Takahashi, A., Homma, T., Ono, M., and Saji, H. (2016) Feasibility of poly (ethylene glycol) derivatives as diagnostic drug carriers for tumor imaging. *J. Controlled Release 226*, 115−123.
(19) Li, W., Chang, Y., Zhan, P., Zhang, N., Liu, X., Pannecouque, C., and De Clercq, E. (2010) Synthesis, In Vitro and In Vivo Release Kinetics, and Anti-HIV Activity of A Sustained-Release Prodrug (mPEG-AZT) of 3′-Azido-3′-deoxythymidine (AZT, Zidovudine). *ChemMedChem 5* (11), 1893−1898.
(20) Antaris, A. L., Chen, H., Cheng, K., Sun, Y., Hong, G., Qu, C., Diao, S., Deng, Z., Hu, X., Zhang, B., et al. (2016) A small-molecule dye for NIR-II imaging. *Nat. Mater. 15* (2), 235.
(21) Baumann, A., Tuerck, D., Prabhu, S., Dickmann, L., and Sims, J. (2014) Pharmacokinetics, metabolism and distribution of PEGs and PEGylated proteins: quo vadis? *Drug Discovery Today 19* (10), 1623−1631.
(22) Nakaoka, R., Tabata, Y., Yamaoka, T., and Ikada, Y. (1997) Prolongation of the serum half-life period of superoxide dismutase by poly (ethylene glycol) modification. *J. Controlled Release 46* (3), 253−261.
(23) Hamidi, M., Azadi, A., and Rafiei, P. (2006) Pharmacokinetic consequences of pegylation. *Drug Delivery 13* (6), 399−409.
(24) Choi, H. S., Nasr, K., Alyabyev, S., Feith, D., Lee, J. H., Kim, S. H., Ashitate, Y., Hyun, H., Patonay, G., Strekowski, L., et al. (2011) Synthesis and In Vivo Fate of Zwitterionic Near-Infrared Fluorophores. *Angew. Chem., Int. Ed. 50* (28), 6258−6263.
(25) Yu, M., Liu, J., Ning, X., and Zheng, J. (2015) High-contrast Noninvasive Imaging of Kidney Clearance Kinetics Enabled by Renal Clearable Nanofluorophores. *Angew. Chem., Int. Ed. 54* (51), 15434−15438.
(26) Yu, M., Zhou, J., Du, B., Ning, X., Authement, C., Gandee, L., Kapur, P., Hsieh, J. T., and Zheng, J. (2016) Noninvasive Staging of Kidney Dysfunction Enabled by Renal-Clearable Luminescent Gold Nanoparticles. *Angew. Chem. 128* (8), 2837−2841.
(27) Huang, J., Li, J., Lyu, Y., Miao, Q., and Pu, K. (2019) Molecular optical imaging probes for early diagnosis of drug-induced acute kidney injury. *Nat. Mater. 18*, 1133.
(28) Rieg, T. (2013) A high-throughput method for measurement of glomerular filtration rate in conscious mice. *J. Visualized Exp.* No. 75, e50330.
(29) Jiang, X., Du, B., Tang, S., Hsieh, J. T., and Zheng, J. (2019) Photoacoustic Imaging of Nanoparticle Transport in the Kidneys at High Temporal Resolution. *Angew. Chem. 131* (18), 6055−6061.
(30) Sano, K., Nakajima, T., Miyazaki, K., Ohuchi, Y., Ikegami, T., Choyke, P. L., and Kobayashi, H. (2013) Short PEG-linkers improve the performance of targeted, activatable monoclonal antibody-indocyanine green optical imaging probes. *Bioconjugate Chem. 24* (5), 811−816.
(31) Tyn, M. T., and Gusek, T. W. (1990) Prediction of diffusion coefficients of proteins. *Biotechnol. Bioeng. 35* (4), 327−338.
(32) Armstrong, J. K., Wenby, R. B., Meiselman, H. J., and Fisher, T. C. (2004) The hydrodynamic radii of macromolecules and their effect on red blood cell aggregation. *Biophys. J. 87* (6), 4259−4270.

DOI: 10.1021/acs.bioconjchem.9b00707
Bioconjugate Chem. 2020, 31, 241−247